Structures 55 (2023) 1447–1459

Contents lists available at ScienceDirect

Structures

journal homepage: www.elsevier.com/locate/structures

Experimental assessment of crack prediction methods in international design codes for edge restrained walls

Karim El Khoury [a], Imogen Ridley [b], Robert Vollum [a,*], John Forth [b], Muhammad Shehzad [b], Abobakr Elwakeel [a], Nikolaos Nikitas [b], Bassam Izzuddin [a]

[a] Department of Civil and Environmental Engineering, Imperial College London, UK
[b] School of Civil Engineering, University of Leeds, UK

A B S T R A C T

Through cracking resulting from external restraint of early-age thermal and long-term shrinkage strain is a significant issue in the construction industry as it causes leakage in water retaining and resisting structures. Concerningly, a recent field study found restraint induced crack widths to frequently exceed crack widths calculated in accordance with UK design practice (BS EN 1992-3 and CIRIA C766). Due to a lack of pertinent data, the reasons for this are uncertain. This paper compares measured and predicted crack widths in a series of 12 full-scale edge restrained walls constructed in the laboratory. The tests examine the influence on cracking of key parameters including concrete mix design, wall reinforcement ratio, wall aspect ratio and relative wall to base cross-sectional area. The measured and calculated crack widths are compared at first cracking and at the end of monitoring. Two types of behaviour were noted in the tests, dependent on when the first cracks formed. Cracking either occurred at early age, within 24 h of stripping the formwork, or later due to restraint of combined early age thermal contraction and shrinkage. The final crack widths were greatest, by a considerable margin, in walls where cracks formed at early age, despite the initial cracks being very narrow. BS EN 1992-3 gives the best estimates of crack width in the two walls that cracked at early age. Crack widths in these walls were significantly underestimated by C766. In the other 10 walls, which cracked later, C766 tends to give the best estimate of crack width.

1. Introduction

At early age (EA), concrete undergoes an exothermal hydration reaction [1] leading to expansion during heating and contraction during cooling. The hydration reaction consumes water [1] generating capillary forces and negative pore pressures. This results in early age autogenous shrinkage [2]. In the longer term (LT), loss of internal moisture to the external environment causes drying shrinkage [3] which continues to develop over many years [4]. If restrained, early age and long term contraction leads to the development of tensile stress. Restraint arises from one part of the element expanding or contracting relative to another [4]. External restraint arises if a member is restrained by previously cast members. Internal restraint is most pertinent to very thick sections, while external restraint dominates in thin elements cast against relatively stiff elements [5,6]. External restraint is classified as end, edge, or a combination of the two [7]. The behaviour of end and edge restrained members is fundamentally different [4,8]. In end restrained members, the axial stiffness reduces on cracking causing a reduction in axial stress throughout the member. The next crack does not form until the axial stress builds up again to the cracking stress. In edge restrained elements, the stress relief from cracking is localised. Schlicke et al. [9] explain that cracking behaviour of an axially loaded RC tie is affected by the number of cracks that have formed and their spacing. Directly after initial cracking, strains are equal in the reinforcement and concrete over large parts of the tie and individual cracks can be considered in isolation. Stabilised cracking is reached when cracks are sufficiently closely spaced to influence each other.

This paper focusses on cracking in edge restrained reinforced concrete walls where stabilised cracking does not usually occur. The tests investigate the influence on cracking of design parameters such as wall and base geometry, concrete mix design and reinforcement arrangement. In the UK, the principal documents used for the assessment of cracking in edge restrained members are BS EN 1992 (Parts 1 (2004) and 3 (2006) [10,11]) and CIRIA Report C766 [4] which provides non contradictory complimentary guidance to BS EN 1992. Despite C766 being based on BS EN 1992 differences in the documents have a notable impact on the calculated crack width. Both documents calculate crack width as the product of the maximum crack spacing, $s_{r,max}$ and crack inducing strain, ε_{cr}, but differences arise in the calculation of the latter. BS EN 1992-3 (2006) takes ε_{cr} as the restrained strain, ε_r, while C766 takes $\varepsilon_{cr} = \varepsilon_r - 0.5\varepsilon_{ctu}$, where ε_{ctu} is the tensile strain capacity of the concrete. The C766 approach is based on the assumption that the tensile

* Corresponding author.
E-mail address: r.vollum@imperial.ac.uk (R. Vollum).

https://doi.org/10.1016/j.istruc.2023.06.087
Received 3 March 2023; Received in revised form 20 April 2023; Accepted 17 June 2023
Available online 30 June 2023

strain in the concrete increases linearly from zero at the crack to ε_{ctu} over $0.5s_{r,max}$ to either side of the crack. Hence, the mean tensile strain in the concrete over $s_{r,max}$ is assumed to be $0.5\varepsilon_{ctu}$. The British Standards Institute version of Eurocode 2 [10,11] gives the same method as the European version [12].

The restrained strain, ε_r, is the fraction R of the free strain, ε_{free}, that is unable to materialize due to restraint. In edge restrained members, BS EN 1992-3 (2006) calculates the restrained strain as $\varepsilon_r = R.\varepsilon_{free}$. Where ε_r is insufficient to cause cracking on its own, its presence reduces the cracking force and, hence, the effective concrete tensile strength [13].

BS EN 1992-3 (2006) states that "restraint factors may be calculated from a knowledge of the stiffnesses of the element considered and the members attached to it". It also provides a set of figures showing restraint factors for common cases of edge restrained walls. The restraint factors in these figures are either 0.5, 0.25 or 0 depending on position. In practice, a blanket value of R = 0.5 is often adopted even though the code allows the use of more refined values.

As in ACI 207.2R-95 [14], C766 calculates the restraint factor at joint level as $R_j = \frac{1}{1+A_{new}.E_{new}/A_{old}.E_{old}}$ in which $A_{new}.E_{new}$ and $A_{old}.E_{old}$ are the axial rigidities of the restrained and restraining elements. In walls of height H and length L, C766 calculates the restraint at height h above the base as follows:

$$R = R_j\left[\left(1.372(h/L)^2 - 2.543(h/L) + 1\right) + 0.044((L/H) - 1.969)(h/H)^{1.349}\right] \quad (1)$$

Below h = 0.1L, C766 considers the closing action of the base slab to control crack widths in the wall. Above 0.1L, R reduces with wall height. Consequently, C766 calculates R, and hence crack width, at a height of 0.1L above the base. C766 also reduces R for creep as described below Table 1.

Table 1
Comparison of BS EN 1992 and CIRIA C766 design equations for restraint induced cracking.

	BS EN 1992	C766
Restraint factor	R = 0.5	Eq. (1)
Restrained strain EA	$\varepsilon_{rEA} = [\alpha_c.T_1 + \varepsilon_{ca}(3)]R$	$\varepsilon_{rEA} = K_{c1}[\alpha_c.T_1 + \varepsilon_{ca}(3)]R_1$
Restrained strain LT	$\varepsilon_r = [\alpha_c(T_1 + T_2) + \varepsilon_{ca} + \varepsilon_{cd}]R$	$\varepsilon_r = \varepsilon_{rEA} + K_{c1}[(\varepsilon_{ca}(28) - \varepsilon_{ca}(3)) + \propto_c.T_2]R_2 + K_{c2}.\varepsilon_{cd}.R_3$
Crack inducing strain	ε_r	$\varepsilon_r - 0.5\varepsilon_{ctu}$
Crack spacing	See Fig. 1	
Design crack width	$w_k = s_{r,max}.\varepsilon_r$	$w_k = s_{r,max}(\varepsilon_r - 0.5\varepsilon_{ctu})$

Note: α_c is the coefficient of thermal expansion for concrete, K_{c1} and K_{c2} are respectively early age and long term creep factors ($K_{c1} = 0.65$ and $K_{c2} = 0.5$), T_1 is the difference between the peak temperature and the ambient temperature at the end of the thermal cycle, T_2 is the difference between the mean ambient temperature at the end of the thermal cycle and the minimum temperature likely to be experienced by the element in its lifetime. $\varepsilon_{ca}(t)$ and $\varepsilon_{cd}(t)$ are the autogenous and drying shrinkage at time t. ε_{ctu} is the tensile strain capacity of the concrete at the time of the crack width calculation. Section 4.9.2 of C766 calculates ε_{ctu} as the ratio of the mean tensile strength (f_{ctm}) to the mean elastic modulus (E_{cm}) at 3 days and 28 days (for early age and long term, respectively). To account for loading duration and creep, ε_{ctu} is multiplied by 1.08 at early age and 1.40 at "late life". C766 tabulates early age and long term tensile strain capacities in terms of aggregate type for a class C30/37 concrete. For cube strengths between 20 and 60 MPa, ε_{ctu} for a C30/37 concrete is multiplied by $0.63 + \frac{f_{ck,cube}}{100}$. Alternatively, ε_{ctu} can be calculated in terms of measured f_{ctm} and E_{cm}. $s_{r,max}$ is the maximum crack spacing in the stabilised cracking stage or twice the transfer length during the crack formation stage.

BS EN 1992-1-1 (2004) provides three formulae for the calculation of the maximum crack spacing, $s_{r,max}$, with the choice of formula dependent on the horizontal reinforcement arrangement. Use of these formulae is summarised in the flow chart of Fig. 1. For horizontal reinforcement spacings satisfying $S \le 5\left(c + \frac{\phi}{2}\right)$, where c is the cover and ϕ the bar diameter, $s_{r,max}$ is calculated using Eq. 7.11 of BS EN 1992-1-1 (2004) (see Fig. 1). In Eq. 7.11, $k_3 = 3.4, k_4 = 0.425, k_1 = 0.8$ for high bond bars, $k_2 = 1$ for direct tension and $\rho_{p,eff} = A_s/(b.h_{c,ef})$ in which A_s is the reinforcement area within width b of the member. For tension members, $h_{c,ef}$ is the lesser of t/2 and 2.5 $\left(c + \frac{\phi}{2}\right)$ where t is the member thickness. C766 takes $k_1 = 1.14$ at early age if the element thickness (t) exceeds 300 mm and the cover (c) is less than 50 mm. If the spacing of the horizontal reinforcement bars is greater than $5\left(c + \frac{\varphi}{2}\right)$, an upper bound to $s_{r,max}$ is given by Eq. 7.14 (see Fig. 1) in which (h-x) is the tensile depth of the section to the neutral axis. For edge restrained members, (h-x) equals the wall height, H, for reasons explained by Beeby [15]. This gives $s_{r,max} = 1.3H$, as defined in BS EN 1992-1-1 (2004), for edge restrained walls with less than minimum horizontal reinforcement.

The BS EN 1992 and C766 methods for calculating crack widths in edge restrained members are summarised in Table 1. The BS EN 1992-1-1 (2004) crack width calculation procedure does not explicitly consider whether or not the restrained strain is greater or less than the concrete cracking strain ε_{ctu} as defined in the Note of Table 1. This is addressed in C766 which defines the cracking 'risk' as the ratio of the crack inducing strain to the tensile strain capacity of the concrete. C766 only calculates restraint induced crack widths if the cracking risk exceeds 1.

BS EN 1992-1-1 (2004) requires the provision of the minimum area of steel given by Eq. (2) in which k_c and k account for the distribution of tensile stress, $f_{c,teff}$ is the effective tensile strength of concrete at first cracking, A_{ct} is the area of concrete in tension before cracking, which for walls restrained along their bottom edge is the total vertical cross sectional area of the wall perpendicular to the horizontal imposed strains, and σ_s is the maximum stress permitted in the reinforcement, which may be taken as the characteristic reinforcement yield strength $f_{y,k}$.

$$A_{s,min} = k_c.k.f_{ct,eff}.A_{ct}/\sigma_s \quad (2)$$

The coefficient $k_c = 1$ for pure tension and k reduces linearly from 1.0 to 0.65 as the section thickness increases from 300 mm to 800 mm.

C766 considers the minimum reinforcement requirements of BS EN 1992-1-1 (2004) to be excessive for edge restrained walls since the opening of cracks is partially restrained by the base. Consequently, C766 reduces $A_{s,min}$ by a multiple $k_{Redge}(= 1 - 0.5R_{edge})$, where R_{edge} is the edge restraint factor at a height of 0.1L. C766 also reduces the concrete tensile strength in Eq. 2 to $0.7f_{ctm}$ where f_{ctm} is the mean concrete tensile strength.

FprEN 1992-1-1 [2], the final draft of the next generation of BS EN 1992-1-1, proposes several changes to the current BS EN 1992 guidance for edge-restraint cracking. The changes are mostly in line with C766. However, unlike C766, FprEN 1992-1-1 [2] evaluates the risk of cracking in edge restrained members by comparing the tensile stress in the concrete $\sigma_{ct}(t)$ to its tensile strength $f_{ctm}(t)$ as proposed in the Coin project [1]. This differs from C766 which compares the tensile strain capacity of the concrete with the restrained strain. C766 uses the full temperature drop T_1 from peak to ambient in the calculation of restrained strain. This is conservative since compressive stress is induced in the restrained element during the heating phase. Subsequently, the restrained stress reverses sign and becomes tensile as the wall cools. Based on Scandinavian practice, the background document [14] to Annex D of FprEN1992-1-1 assumes by default that only 90 % of the peak temperature drop T_1 causes tensile stress. FprEN 1992-1-1 calculates crack spacing similarly to BS EN 1992-1-1 (2004) (Eq. (7.11)) but with amended coefficients replacing k_{1-4} in Eq. 7.11. The crack width is calculated with Eq. (4) in which $k_w = 1.7$ converts the mean crack width

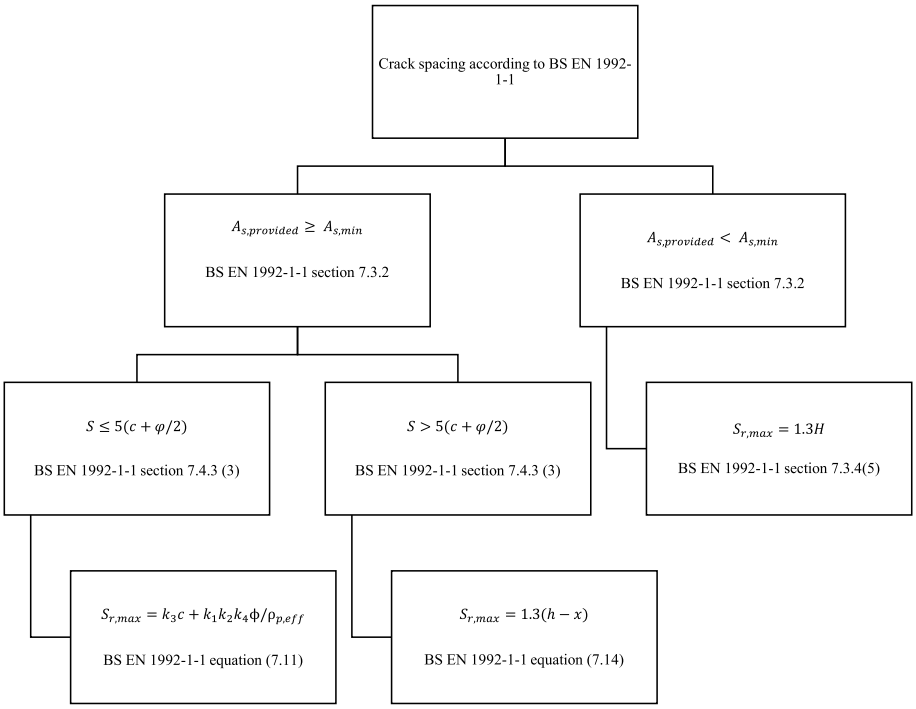

Fig. 1. Flow chart for the calculation of crack spacing as per BS EN 1992-1-1 (2004).

into a calculated one and $k_{1/r}$ accounts for curvature. The mean crack spacing $s_{rm,cal}$ is limited to a maximum of $1.3(h-x)/k_w$.

$$w_{k,cal} = k_w.k_{1/r}.s_{rm,cal}.\varepsilon_{cr} \quad (4)$$

In edge restrained elements, FprEN 1992-1-1 calculates ε_{cr} similarly to C766, but 40 % of the concrete cracking strain, ε_{ctu}, is subtracted from ε_r compared with 50 % in C766. Finally, a restraint factor of R = 0.5 is recommended despite the background document [16] acknowledging the variation in restraint with time and referring to the formulation proposed by CIRIA C660 [17]. Due to the similarity of the treatment of restraint induced cracking in C766 and FprEN 1992-1-1, the latter is not considered further in this paper.

This research was motivated by previous work [6,18], which showed BS EN 1992 not to properly capture the observed cracking behaviour in edge-restraint elements. This conclusion is supported by Jędrzejewska et al. [19], who found restraint induced crack widths in numerous structures to exceed crack widths calculated with BS EN 1992 and C766 on multiple occasions. They concluded that a re-evaluation of design guidance is required with C766 most pressing as it predicts lower crack widths than BS EN 1992. The adverse impact of cracking in concrete structures resulting from shrinkage, thermal and restraint effects, including the potential durability, functionality, aesthetic and economic consequences is widely discussed across the literature [20,21]. This paper evaluates the accuracy of crack width calculation methods in BS EN 1992 and C766 by comparing measured and calculated crack widths in 12 edge restrained walls constructed at UoL and ICL.

2. Experimental details

The work presented here is part of an experimental campaign into restraint induced cracking being undertaken at University of Leeds (UoL) and Imperial College London (ICL). Results from 12 tests in which RC walls were cast onto existing, mature base slabs are presented and discussed in this paper. The experimental procedure is explained below.

2.1. Test Set-Up

The base and wall construction sequence adopted at ICL is illustrated in Fig. 2(a) to (d). A similar procedure was adopted at UoL apart from the use of modular formwork panels. The ends of the base were tied down to the laboratory floor with a pair of holding down bolts to prevent curling. The bolts were prestressed to a load of 100kN prior to casting the wall. The wall was cast a minimum of 28 days after the base which restrained the wall. Control specimens were cast alongside each base and wall to determine pertinent concrete properties such as free shrinkage strain, free thermal strain and tensile strain capacity. The control specimens included an unreinforced 1 m square trial panel with the same thickness as the wall.

The specimen dimensions and reinforcement details varied between tests as shown in Table 2. Walls UoL1-5 and ICL1 had a length to height ratio (L/H) of 4, while L/H for ICL2-7 was 5.2. The base to wall area ratio (A_b/A_w) was 0.83 for UoL1 and ICL1 with base slab thickness 0.3 m, wall thickness 0.25 m and wall height 1.3 m. Since walls ICL1 and UoL1 did not crack, A_b/A_w was increased in subsequent tests. The wall thickness was 0.25 m in all the tests except ICL6-7 where the thickness was reduced to 0.175 m to promote early age cracking. In walls UoL2-5, the base thickness and width were increased to 0.4 m and 1 m, respectively, while the wall height was reduced to 1 m, thus achieving A_b/A_w of 1.6. In walls ICL2-7, the wall height was 1.025 m, and base thickness 0.3 m thus increasing A_b/A_w to 1.05 for ICL2-5 and 1.51 for ICL6-7. Walls ICL2-4 had 0.25 m square openings positioned just above the base with far edge at 0.6875 m from each end of the wall. These openings were provided to enable the walls to be loaded, at the end of the test, horizontally in direct tension through a cross member. The ends of ICL2-3 were increased in height to 1.3 m over a length of 0.7 m to provide a reaction to the top strut of the loading rig as described in [22].

In all specimens, the top and bottom reinforcement in the base consisted of longitudinal 12 mm bars at 100 mm spacing and transverse 10 mm bars at 300 mm spacing. Table 3 gives details of the horizontal and vertical reinforcement provided in each wall. The horizontal bars in the wall were in the outer layer. The effect of omitting horizontal reinforcement altogether was investigated in walls UoL4 and UoL5. Also

Fig. 2. Test set up for ICL2 showing a) Reinforcement of wall and base before casting, b) Instrumentation, c) Installation of formwork before casting of wall and d) Wall after striking of formwork.

Table 2
Dimensions of bases and walls.

Wall	Base dimensions (m)			Wall dimensions (m)			A_b/A_w
	W	T	L	H	T	L	
ICL1	0.9	0.3	6.0	1.3	0.25	5.2	0.83
ICL2-5	0.9	0.3	6.0	1.025	0.25	5.2	1.05
ICL6-7	0.9	0.3	6.0	1.025	0.175	5.2	1.51
UoL1	0.9	0.3	6.0	1.3	0.25	5.2	0.83
UoL2-5	1.0	0.4	5.4	1.0	0.25	4.0	1.60

shown in Table 3 are the minimum areas of horizontal reinforcement required by BS EN 1992-1-1 (2004) and C766 calculated in terms of the 28 day concrete tensile strength. The latter was taken as 0.9 times the splitting strength as recommended by BS EN 1992-1-1 (2004). The minimum areas of reinforcement required by C766 and BS EN 1992-1-1 (2004) are also compared graphically in Fig. 3 for both early age and long term. Early age depicts early age conditions up to 3 days from casting as defined in C766 [4], while long term depicts conditions at the end of each test. The early age minimum reinforcement areas in Fig. 3 were calculated with measured concrete tensile strengths at 3 days and are pertinent to control of early age cracking.

Based on trial mixes at UoL, the concrete mix design was refined as the tests progressed in order to increase the likelihood of cracking. To maximise the temperature rise, and hence likelihood of cracking, CEM1 was specified without any cement replacement. Limestone coarse aggregate was initially used but to increase the coefficient of thermal expansion (CTE) this was later changed to gravel at ICL and sandstone at UoL (see Table 4). With the exception of UoL1, the shuttering for the walls was insulated to maximise the thermal drop following casting. At ICL, the shuttering consisted of 19 mm plywood sheets spanning between 145x70 mm^2 horizontal timber joists spaced at 250 mm centres. The plywood between the joists was insulated with either 50 mm or 100 mm polyisocyanurate (PIR) sheets placed between the joists as well as the top and ends of the wall. In walls ICL1-5, the surface conductance of the provided 19 mm plywood and 50 mm PIR sheets is estimated to be 0.42 W/m^2K. In walls ICL6 and ICL7, the thickness of the PIR was increased to 100 mm reducing the thermal conductance to 0.21 W/m^2K. Modular technopolymers-based formwork panels were used at UoL in combination with sheep wool insulation, aside from UoL1 where insulation was omitted. In walls UoL2-4, 100 mm of insulation provided a total surface conductance of 0.49 W/m^2K. This was increased to 200 mm for UoL5, giving 0.22 W/m^2K surface conductance. The formwork for the 1 m square trial panels was insulated similarly to the walls.

2.2. Monitoring procedure

Temperature was measured with K-type thermocouples in the base, wall and trial panel following casting. The thermocouples were positioned evenly over the height of each element at its centre, quarter-length and ends. Temperature readings were recorded every minute at early age with the frequency of measurements reduced to hourly in the

Table 3
Details of the reinforcement.

Test	Wall reinforcement								
	Vertical bars		Horizontal bars		Cover (mm)	f_{ct}(28d) for A_{smin} (MPa)	ρ_h prov-ided (%)	$\rho_{h,min\ LT}$ BS EN 1992-1-1 (2004) (%)	$\rho_{h,min\ LT}$ C766 (%)
	ϕ (mm)	Spac-ing (mm)	ϕ (mm)	Spac-ing (mm)					
ICL1	16	150	10	180	40	3.1	0.35	0.61	0.35
ICL2	16	150	16	180	25	2.9	0.89	0.58	0.32
ICL3	12	180	16	180	25	2.8	0.89	0.57	0.32
ICL4	12	180	10	300	30	2.6	0.21	0.52	0.29
ICL5	12	180	10	180	30	2.7	0.35	0.53	0.30
ICL6	12	180	10	300	25	2.7	0.30	0.54	0.29
ICL7	12	180	10	180	25	2.0	0.50	0.41	0.22
UoL1	16	150	10	180	30	3.4	0.35	0.68	0.40
UoL2	16	150	10	180	30	1.7	0.35	0.35	0.19
UoL3	20	125	10	180	30	2.2	0.35	0.43	0.23
UoL4	12	180	0	0	0	2.6	0.00	0.51	0.27
UoL5	20	170	0	0	0	2.9	0.00	0.58	0.31

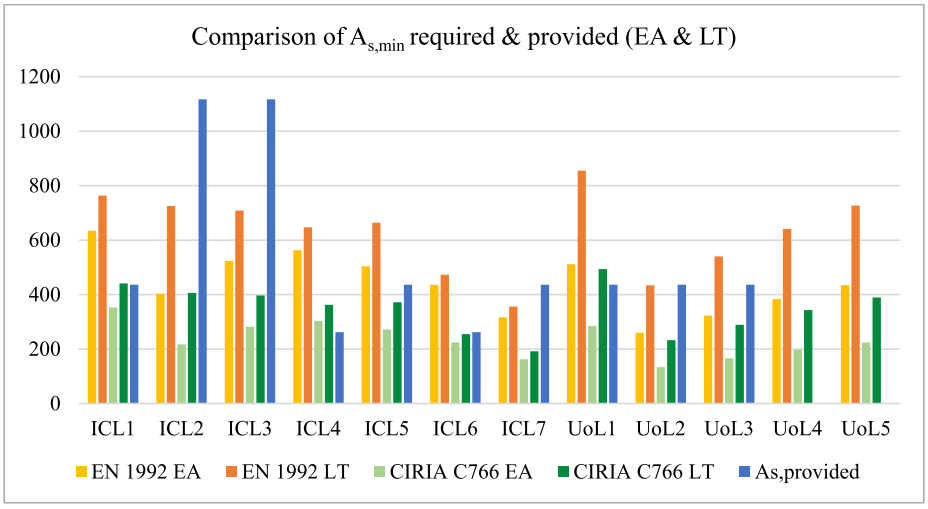

Fig. 3. Comparison of $A_{s,min}$ required (at EA & LT) & provided.

Table 4
Measured 28 day properties.

	Aggregate type	CTE	f_{cm} (MPa)	f_{ctm} (MPa)	E_{cm} (GPa)	T_1 ($t \leq 3$ days) from peak (used in crack width calculation) (°C)	T_{1D} ($t \leq 3$ days) from 1st DEMEC reading (°C)	T_{1D}/ T_1
ICL1	Limestone	8.45	51.8	3.1	35.7	34.9/18.0 hrs	32.9/20.5 hrs	0.94
ICL2	Limestone	8.45	42.6	2.9	30.9	34.7/17.9 hrs	31.3/18.5 hrs	0.90
ICL3	Limestone	8.45	42.5	2.8	31.9	40.5/17.6 hrs	36.0/18.4 hrs	0.89
ICL4	Gravel	12.2	41.3	2.6	30.5	30.7/20.9 hrs	25.3/21.8 hrs	0.82
ICL5	Gravel	12.2	42.2	2.7	32.9	30/22.1 hrs	24.9/23.1 hrs	0.83
ICL6	Gravel	12.2	40.9	2.7	37.3	43.9/20.8 hrs	38.2/22.0 hrs	0.87
ICL7	Gravel	12.2	29.4	2.0	31.4	36.8/20.4 hrs	31.8/21.9 hrs	0.86
UoL1	Limestone	9.0	49.4	3.4	31.4	27.7/17.8 hrs	27.0/20 hrs	0.97
UoL2	Limestone	9.0	30.9	1.7	29.9	24.3/18.8 hrs	17.5/20 hrs	0.72
UoL3	Sandstone	12.5	35.3	2.2	22.1	35.5/19.5 hrs	33.2/18.8 hrs	0.94
UoL4	Sandstone	12.5	35.9	2.6	24.2	25.7/19.0 hrs	22.9/20.2 hrs	0.89
UoL5	Sandstone	12.5	41	2.9	22.8	40.2/17.8 hrs	29.9/20.5 hrs	0.74

long term. Surface strains were measured in one face of the base, wall and trial panel over a regular grid of demountable mechanical strain gauge (DEMEC) points [22]. The DEMEC grid for the walls consisted of horizontal rows of DEMEC points, positioned over the complete length of the wall. At ICL, the rows were positioned at 250 mm centres vertically, while UoL adopted 7 rows at a 150 mm vertical spacing. Over the central half of the wall a gauge length of 200 mm was adopted at UoL and 250 mm at ICL. Over the end quarters of each wall, the gauge length was doubled to 400 mm at UoL and 500 mm at ICL. The peak temperature typically occurred immediately before removal of formwork which was commenced once the temperature had peaked. At ICL one side of the formwork was initially removed to allow the DEMEC points to be fixed. At UoL the modular panels of the formwork were removed sequentially as the DEMEC points were fixed. The first full set of DEMEC readings in the wall and trial panel was typically taken around one hour after stripping the formwork (see Table 4). The formwork was removed from the other wall face while the first set of DEMEC readings was being taken at ICL, and immediately after the first set of

readings at UoL. In the other face of the walls, strain was measured using digital image correlation. Good correlation was achieved between the strains measured in each face of the walls. The measured strain can be subdivided as follows:

$$\varepsilon_{measured} = \varepsilon_{total} = \varepsilon_{free} + \varepsilon_r + w/L \quad (5)$$

in which the free strain $\varepsilon_{free} = \alpha.\Delta T + \varepsilon_{sh}$ where α is the CTE, ΔT is the temperature drop in the wall from the first set of DEMEC readings, ε_{sh} is the shrinkage strain, ε_r is the restrained strain, w is the crack width if present and L is the gauge length over which the strain is measured. Tensile creep [23] increases the measured strain $\varepsilon_{measured}$ and, therefore, the restrained tensile strain ε_r which includes an elastic and creep component.

The estimated restrained strain in the concrete (ε_r) before cracking is given by:

$$\varepsilon_r = \varepsilon_{measured} - \varepsilon_{free} \quad (6a)$$

After cracking, the estimated restrained strain in the concrete is given by:

$$\varepsilon_r^{'} = \varepsilon_{measured} - \varepsilon_{free} - w/L \quad (6b)$$

The restrained strain was estimated with equation (6a) throughout the tests even if cracking had occurred. Strains were determined between each pair of DEMEC points and then averaged over the central half of the wall for each row. The resulting strain $\varepsilon_{r,ave}$ includes the crack strain and hence exceeds the tensile strain in the concrete between cracks. The difference between $\varepsilon_{r,ave}$ and $\varepsilon_r^{'}$ is given by:

$$\varepsilon_{r,ave} - \varepsilon_r^{'} = \frac{\sum_1^n w_i}{0.5L_{wall}} \quad (7)$$

where n is the number of cracks of width w_i within the central half of the wall of length $0.5L_{wall}$.

The influence of cracking on $\varepsilon_{r,ave}$ increases with crack width and number of cracks. For a single crack of width 0.02 mm in $0.5L_{wall}$ equal to 2.6 m, $\varepsilon_{r,ave} - \varepsilon_{r,ave}^{'}$ equals 8 με. This increases to 58 με for 3 cracks with combined width 0.15 mm. Consequently, once the wall has cracked significantly the experimentally derived restrained strains are no longer directly comparable with $\varepsilon_r = R.\varepsilon_{free}$ as calculated in BS EN1992-3 (2006).

The free shrinkage strain in the walls was estimated using either published guidance (ICL1 and UoL1-3) or from strains measured in the trial panels after correction for thermal strain where available (ICL2-7 and UoL4-5). The thermal strain was estimated as the product of the CTE and the measured temperature drop from the first set of DEMEC readings. The CTE was determined experimentally at ICL from strain measurements in prisms heated in a water bath. For ICL1 and UoL1-3, without trial panels, shrinkage strains were measured in small scale prisms and then compared with those given by the guidance documents BS EN 1992-1-1 (2004) [10] and Model Code 2010 [24]. Additionally, UoL made comparisons with shrinkage models B4 Bazant [25] and ACI 209.2R [26]. Shrinkage in these walls was calculated with the best matching model. The experimentally derived shrinkage strains from the top row of the trial panels were adopted for walls ICL2-7 and UoL4-5. The walls were regularly inspected with a magnifying glass to identify the development of cracks. At the onset of cracking, and at regular intervals thereafter, crack widths were measured using a portable microscope with 40x magnification and measuring resolution of 0.02 mm. The crack development and the location of the maximum crack width were recorded for each crack.

3. Results and discussion

3.1. Measured concrete properties and temperatures

Table 4 summarises the measured 28-day concrete properties for each wall. The ICL CTEs in Table 4 are measured whilst those given for the UoL tests are taken from C766 according to aggregate type. The concrete compressive strengths (f_{cm}) were determined from 100 mm diameter cylinders at ICL and 150 mm diameter cylinders at UoL. The concrete tensile strengths (f_{ctm}) were taken as 90 % of the measured 150 mm diameter split cylinder strengths as recommended by BS EN 1992-1-1 (2004) [10]. Fig. 4, which is representative, shows the variation with time of the temperature profile at the centre of the wall over its height. The temperature drop (T_1) from peak to ambient at 3 days varied between walls as shown in Table 4 which also shows the time in hours from end of casting the wall to i) the peak temperature and ii) the first set of DEMEC readings. The temperature drop to ambient at 3 days from the time of the first set of DEMEC readings is depicted T_{1D}. The variation in T_1 between walls is a function of differences between walls in concrete mix design, insulation, striking time and ambient temperature. In all walls, the maximum temperature developed in the central region of the wall, between 50 and 80 % of the wall height above the base. The drop in temperature, over the wall height, between mid-height of the wall and the base is due to heat being lost to the base.

3.2. Restrained strains and development of cracking

Of the 12 walls reported here, 10 cracked at some point during their monitoring period. Tables 5 and 6 give the free strain, the restrained strain, the concrete tensile strain capacity, wall age and maximum crack width at i) first cracking and ii) the end of monitoring. Additionally, Table 5 shows the height of crack width measurement above the base when it first formed and Table 6 shows the shrinkage strain in the wall at end of monitoring. Walls ICL1 and UoL1-2 are omitted from Table 5 since they did not crack. The C766 restrained strains in Tables 5 and 6 are the product of the free strain and the restraint factor calculated with

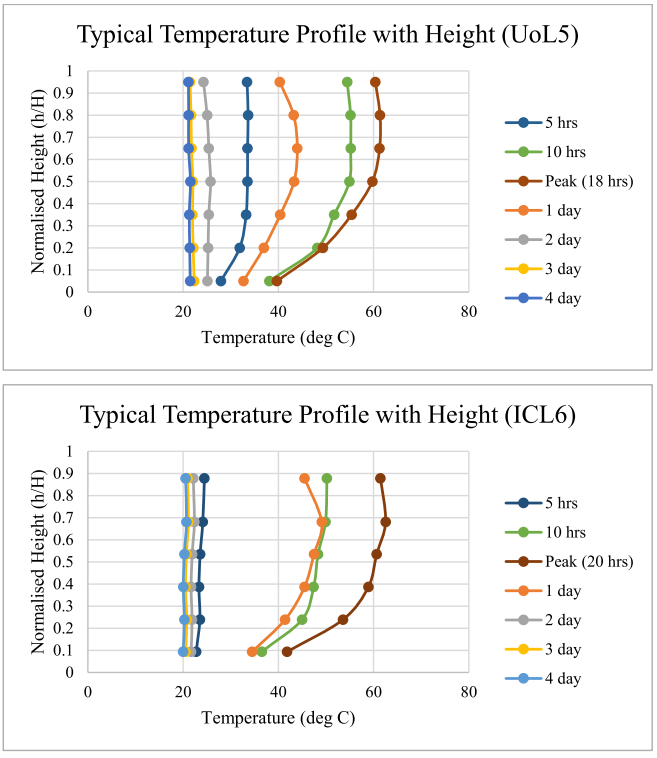

Fig. 4. Typical Temperature Profile with Time (UoL5 and ICL6).

Table 5
Initial cracking.

Test	Age (t) at cracking (days)	$\varepsilon_{free,max}$(t) (test)	ε_{free}(t) from peak (C766)	ε_{ctu}(t) (C766)	$\varepsilon_{r,ave}$(t) max (test)	ε_r(t) (C766)	Crack width w (mm)	Height at w (mm)
ICL2	10	315	377	118	75	105	0.10	243
ICL3	7	335	395	107	86	108	0.04	410
ICL4	19	396	458	115	114	127	0.02	340
ICL5	20	407	454	110	121	126	0.02	383
ICL6	1.14	289	328	102	94	111	0.02	390
ICL7	1.17	247	335	85	66	113	0.04	390
UoL3	50	478	572	140	128	190	0.04	390
UoL4	46	347	443	151	123	141	0.06	350
UoL5	21	560	629	174	201	210	0.04	280

Table 6
Final Cracking (end of monitoring period).

Test	Age (t) at end of monit-oring (days)	ε_{ctu}(t) (C766)	$\varepsilon_{sh,net}$(t)†	$\varepsilon_{sh,wall}$(t)	$\varepsilon_{free,max}$(t) (test)	Max $\varepsilon_{r,ave}$(t) (test)	ε_r(t)(C766)	Max crack width test w (mm)
ICL1	112	125	156	229	511	150	111	–
ICL2	87	137	304*	335*	559	247	151	0.12
ICL3	78	129	69*	296*	588	196	120	0.10
ICL4	70	123	126*	182*	525	150	140	0.04
ICL5	71	118	147*	211*	516	148	142	0.06
ICL6	111	106	336*	400*	815	469	263	0.38
ICL7	113	95	390*	453*	857	448	244	0.40
UoL1	50	156	88	139	382	96	86	–
UoL2	50	83	95	144	301	179	106	–
UoL3	100	143	140	196	611	101	201	0.14
UoL4	73	154	180*	235*	521	100	166	0.08
UoL5	73	185	286*	341*	715	583	260	0.10

* Experimentally determined shrinkage based on trial panels.
- No cracking observed.
† Differential shrinkage between base and wall.

equation (1) at a height of 0.1L and adjusted for creep as described in the notes below Table 1. The thermal component of the free strain was calculated in terms of the peak temperature drops T_1 given in Table 4. The reference time for the "test" strains in Tables 5 and 6 is that of the first set of DEMEC readings which accounts for the "test" free strains in Table 5 being less than the C766 free strains. The temperature drop T_2 (see Table 1) was neglected in the long term C766 calculations since there was no significant temperature difference between the base and wall after 3 days. The thermal component of the "test" long term free strains in Table 6 includes that due to T_2 since this impacted the measured DEMEC strains. Average restrained strains were calculated over the central half of each wall for each row of DEMEC points, in terms of the corresponding measured temperature drop in that row. The greatest of the row averages is reported as $\varepsilon_{r,ave}(t)$ "test" in Tables 5 and 6. At first cracking, $\varepsilon_{r,ave}(t)$ was greatest in the second row of DEMEC points above the base in ICL2-7 corresponding to a height of around 0.1L above the base as assumed in C766. For UoL3-5, the maximum $\varepsilon_{r,ave}(t)$ fell between 0.05L and 0.13L above the base. Uncertainties arise in the experimentally derived restrained strains due to i) cracking occurring between sets of DEMEC readings and ii) assuming the wall to be unstressed when the first set of DEMEC readings is taken. Between striking and taking the first set of DEMEC readings, typically around an hour later (see Table 4), the maximum temperature in the wall dropped between 10 and 14 % at ICL with the exception of walls ICL4-5 where the drop was ~17 %. At UoL, the corresponding temperature drop varied between 3 % and 28 %. The temperature drops from peak (T_1) and from taking the first set of DEMEC readings (T_{1D}) are shown in Table 4 along with the corresponding time in hours from casting. Consequently, with a few exceptions, assumption ii) is broadly consistent with Scandinavian practice [14] which assumes 90 % of the temperature drop to contribute to the development of tensile stress. The experimental restrained strains in Table 6 were calculated with equation (6a) which neglects the influence of cracking which becomes progressively more significant as cracking develops. This explains why the experimental restrained strains in Table 6 at end of monitoring are typically significantly greater than calculated with C766.

The C766 concrete tensile strain capacity ε_{ctu}(t) was estimated in terms of f_{ctm}(t) and E_{cm}(t) using the approach described in the notes below Table 1. The concrete properties f_{ctm}(t) and E_{cm}(t) were estimated by multiplying the measured 28 day values by the age adjustment factor β(t) given in EN 1992-1-1 (2004). The tensile strain capacity at the time of cracking was calculated as $\varepsilon_{ctu}(t) = k_{C766}.\frac{f_{ctm(t)}}{E_{cm(t)}}$, where k_{C766} is taken as 1.08 at an age of up to 3 days like for ICL6-7 and 1.40 for ages beyond 28 days like for UoL3-4. Linear interpolation was applied when cracking occurred between 3 and 28 days as observed in ICL2-5 and UoL5. Table 5 shows that the C766 restrained strains at first cracking were similar to or greater than $\varepsilon_{ctu}(t)$ in all the walls that cracked. At first cracking, the experimental restrained strains lie between 76 and 123 % of the C766 tensile strain capacity ε_{ctu}. The deviations between the two are unsurprising given the approximations involved in the calculation of each.

Walls ICL6 and ICL7, which were the only walls to crack at early age, cracked within 1 day of casting. Walls ICL2-ICL5 and UoL5 all cracked prior to 28 days, while UoL3 and UoL4 cracked notably later at 50 and 46 days, respectively. The variation in age at which cracking initially occurred is a result of differences in the development of concrete tensile strength and restrained strain with time. In walls ICL6 and ICL7, the restrained early age thermal strain was sufficient to cause cracking but in the other walls, cracking resulted from the combined effect of the early age thermal drop and long term shrinkage.

Within one week of initial cracking, further short fine cracks formed in each wall. Subsequently, the first cracks to form widened and lengthened. The cracks tended to develop in short unconnected lengths which subsequently joined forming wider cracks that extended over the wall height. Cracks were typically near vertical apart from near the wall ends where cracks were inclined as shown in Fig. 5. In walls ICL2-ICL4 with openings, wide diagonal cracks initiated at the top outer corner of the opening which acted as a crack inducer.

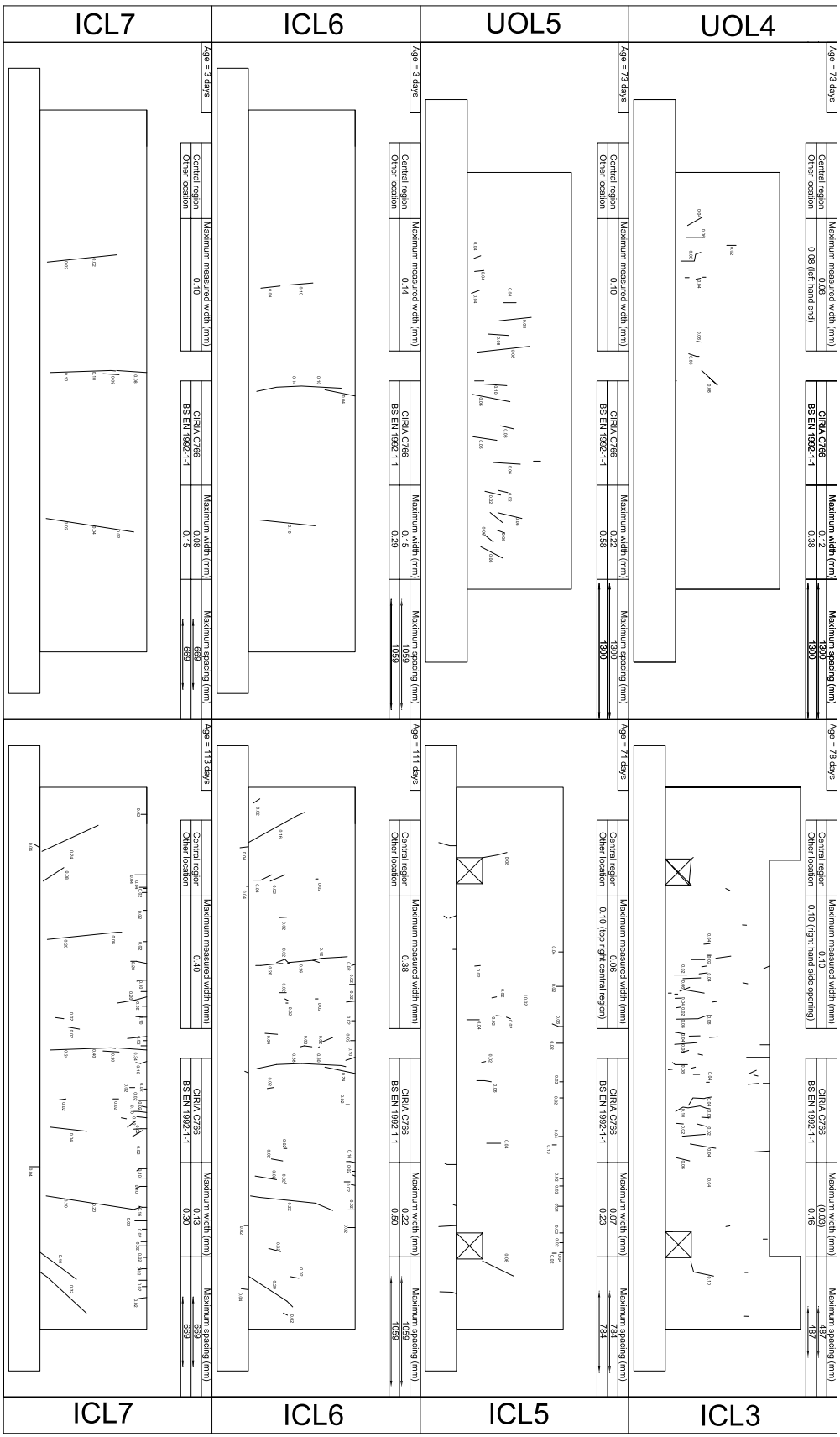

Fig. 5. Representative experimental cracked walls (ICL and UOL).

Table 5 gives the maximum early age crack width and corresponding height above the base. The maximum crack width at the end of the monitoring period is reported in Table 6. The corresponding crack patterns are shown in Fig. 5. The crack patterns in walls ICL6 and ICL7, which cracked at early age, are fundamentally different from those in the other cracked walls. The main cracks in ICL6 and ICL7 are through cracks, which extend over the full height of the wall at a spacing of approximately the wall height of 1 m. Fewer secondary cracks formed in walls ICL6 and ICL7 than typically in the other walls. The initial early age cracks in walls ICL6 and ICL7 increased in width during the monitoring period from 0.02 mm to 0.38 mm in ICL6 and 0.04 mm to 0.40 mm in ICL7. These increases in width are the largest observed. In the remaining walls that cracked, the cracks were shorter, narrower and more closely spaced. Final cracking in walls ICL2, 3 and UoL5 was much more extensive than in walls ICL4, UoL3 and UoL4.

Fig. 6a and b depict the location and severity of cracking in all the walls in the form of heat maps which show the total number of cracks in each grid square, summed over all the walls, and the maximum crack width in each grid square. The heat maps highlight the trends in the crack patterns of Fig. 5. As the crack widths were manually recorded, they are not available for all positions for every crack. Therefore, the heat maps in Fig. 6 are indicative, showing the maximum known crack width in each grid location. Fig. 6a shows that cracking tended to be concentrated in the lower half of the walls with more cracks forming in the central region of the walls than towards the ends. This is consistent with the diagrams of edge restraint factors in BS EN1992-3 (2006). The greatest number of cracks formed between 15 and 45 % of the wall height above the base and between 35 and 75 % of the wall length from its end. For the tests presented here, a maximum of 5 cracks formed in any cell of the bottom row of the grid. The maximum number of cracks in a cell is 19 at 40 % of the wall height which is just below a height of 0.1L.

Up to a height of 0.1L, which for the tested walls corresponds to between 40 % and 51 % of the wall height, C766 suggests the presence of the base slab generates a closing action on the cracks. Below this height, C766 suggests cracks will be narrower. Midway along the wall, immediately above the base slab, the maximum crack width was 0.24 mm which is 60 % of the maximum measured crack width which occurred between 40 and 60 % of the wall height above the base. Fig. 6b suggests that the assumption of C766 that the maximum crack width occurs at a height of 0.1L above the base is reasonable even though cracks were relatively wide below that level. Fig. 6a shows that numerous short closely spaced fine cracks formed at the top of the wall. The cause of these cracks is uncertain but a possible explanation may lie in the concrete at the top of the pour being weak due to segregation. This combined with internal restraint from the reinforcement is a possible cause of the cracking. It should be noted that at UoL, the test set-up did not allow visual monitoring of cracking at the top of the wall.

3.3. Comparison of experimentally-observed and code-predicted cracking behaviour

"Experimental" crack widths were calculated in each wall using the crack width calculation methods of C766 and BS EN1992 (Part 1 and 3) described in the introduction to this paper and detailed in Table 1. The material properties, shrinkage and early age temperature drop T_1 from peak, used in the calculations were the experimentally derived ones given in Table 4. A restraint factor of R = 0.5 was adopted for calculations with BS EN 1992. The restrained strains used in the calculation of C766 crack width (depicted $\varepsilon_r(t)$ (C766)) were taken from Table 5 at early age and Table 6 for the long term. The long term temperature drop T_2 was taken as zero in the crack width calculations since there was no significant temperature differential between the wall and base. In crack width calculations to BS EN 1992-1-1 (2004), the free long term drying shrinkage was taken as that in the wall, unless stated otherwise, since the code defines the free strain as "the strain which would occur if the member was completely unrestrained". In applying C766, the contribution of long term drying shrinkage to the free strain was taken as the differential strain between the wall and base slab from the time of casting the wall.

Maximum crack spacings $s_{r,max}$ were calculated in accordance with BS EN 1992-1-1 (2004) for each wall. The results are presented in Table 7 which shows $s_{r,max}$ calculated i) with equation 7.11 of BS EN 1992-1-1 (2004) (C766) and ii) in accordance with the flow chart of

Table 7
Calculated crack spacing.

Test	BS EN 1992-1-1 (2004)		
	$s_{r,max}$ (mm)	Clause	$s_{r,max}$ Eq. 7.11 (mm)
ICL1	1690	7.3.4(5)	1013
ICL2	1333	7.14	487
ICL3	1333	7.14	487
ICL4	1333	7.3.4(5)	1238
ICL5	1333	7.3.4(5)	784
ICL6	1333	7.3.4(5)	1059
ICL7	1333	7.3.4(5)	669
UoL1	1690	7.3.4(5)	784
UoL2	1300	7.14	784
UoL3	1300	7.14 (EA), 7.3.4(5) (LT)	784
UoL4	1300	7.3.4(5)	1300
UoL5	1300	7.3.4(5)	1300

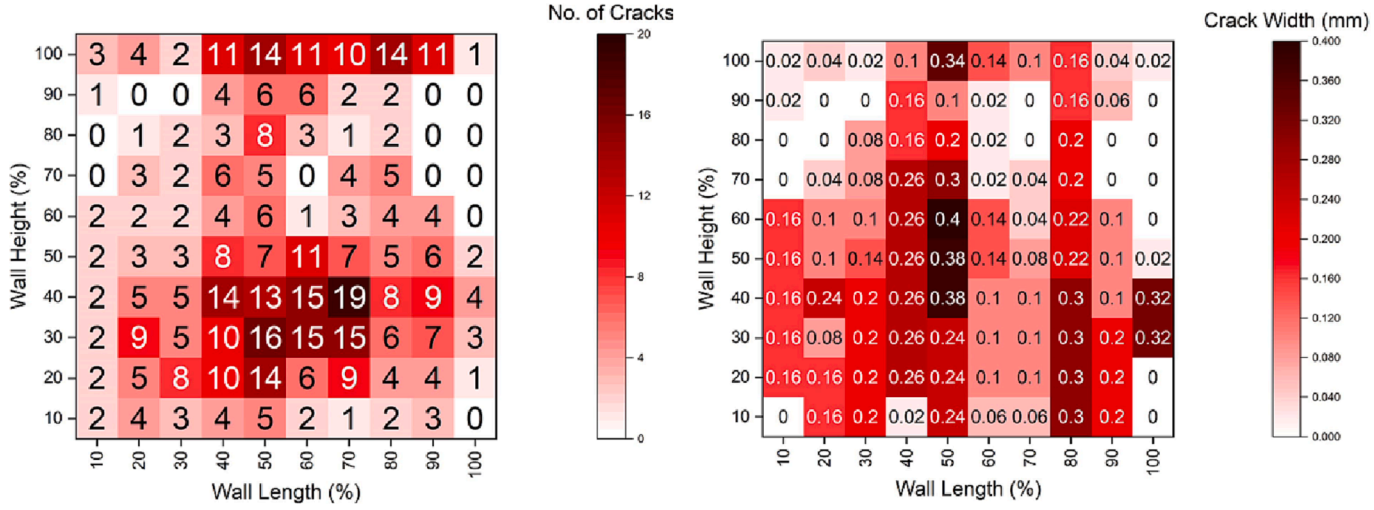

Fig. 6. Heat maps showing a) crack occurrence and b) maximum crack width registered across all walls.

Fig. 1 for bar spacings greater than 5(c + 0.5ϕ) (BS EN 1992-1-1 (2004)). The limit of 5(c + 0.5ϕ) was marginally exceeded in walls ICL2, ICL3, ICL5 and ICL7 and significantly in walls ICL4 and ICL7. Table 2 shows that walls ICL1, ICL4-ICL6, UoL1 and UoL4-UoL5 had less than the minimum area of horizontal reinforcement required by BS EN 1992-1-1 (2004) but with the exception of UoL4 and UoL5, which had none, all the walls had more horizontal reinforcement than required by C766. In walls with either $A_{s,min}$ below that given by equation (2) or horizontal bar spacing greater than 5(c + 0.5ϕ), $s_{r,max} = 1.3H$ according to BS EN 1992-1-1 (2004).

Table 8 shows crack widths calculated using C766 and BS EN 1992 (2004) at early age and long term. For purposes of comparison, the crack widths in Table 8 were calculated with $s_{r,max}$ from equation 7.11 of BS EN 1992-1-1 (2004) with the exception of UoL4-5, without horizontal reinforcement, where $s_{r,max} = 1.3H$. In C766, the crack width is not calculated at early age when the risk of cracking is below 1. In this case, the crack width is depicted "N/A", whereas a long term value is provided in brackets if cracking is not predicted.

Fig. 7 shows the measured and calculated development of crack width with time in walls ICL2, ICL4, ICL6 and ICL7. The influence of using the full, instead of differential, free shrinkage strain in the BS EN 1992-1-1 (2004) crack width calculations is small for the tested walls. This is illustrated in Fig. 7 where "EN 1992 A" and "EN 1992 B" depict crack widths calculated with full and differential shrinkage respectively. Fig. 7 shows a steady increase in the calculated crack widths with time whereas the measured crack widths tend to increase in more discrete steps but this may be due to limitations in the resolution of the crack microscope. Calculating $s_{r,max}$ using the procedure given in Table 1, rather than equation 7.11, leads to an increase in crack spacing (see Table 7), and hence maximum crack width, of between 8 % and 174 %.

Walls UoL1-2 and ICL1 did not crack. C766 correctly predicts UoL1 and ICL1 not to crack but falsely predicts UoL2 to crack. In UoL2, the calculated restrained strain exceeds the C766 early age and long term tensile strain capacities by 80 % and 20 % respectively. C766 overestimates crack widths in ICL4 and UoL4-5 by between 50 % and 125 %. More concerningly, C766 underestimates the maximum long term crack width in walls ICL2, 3, 6, 7 and UoL3 by between 42 and 80 %. Underestimation of crack width is particularly undesirable since it can lead to water leakage in water retaining and resisting structures. The underestimate in crack width is particularly pronounced for walls ICL6 and ICL7 where early age cracking occurred. As shown in Table 2, the area of horizontal reinforcement provided in walls ICL6 and ICL7 satisfied the minimum requirements of C766. In ICL7, the minimum reinforcement requirement of BS EN1992 was also satisfied.

The BS EN 1992-1-1 (2004) crack widths in Table 8, calculated with $s_{r,max}$ from Eq. 7.11, exceed all the measured crack widths, apart from ICL7, by mostly a wide margin. The overestimate in crack width is largely due to the experimental restraint factor being significantly less than the default value of 0.5 used in the BS EN 1992 calculations. This is evident in Table 9 which compares the experimental restraint factors (RF) with the equivalent factors used in C766. The restraint factors are compared at 3 days, first cracking and end of monitoring. The C766 RFs are composite ones calculated as $RF = \frac{\varepsilon_r}{\varepsilon_{free}}$ in which ε_r and ε_{free} are the C766 restrained and free strains presented in Tables 5 and 6 at first cracking and end of monitoring. The experimental restraint factors are average values calculated over the central half of the wall at heights of 0.08L and 0.125L. The measured and calculated maximum RF values are broadly similar at early age and first cracking for walls ICL1-5, UoL1 and UoL5. In walls ICL6-7 the measured long term RFs are significantly greater than calculated with C766 due to the effect of cracking as explained in Section 2.2. The measured RFs for UoL2 (which did not experience cracking) are also noticeably higher than given by C766 at both early-age and long term conditions, while for UoL3-4 the experimental RFs fall below the predictions of C766.

The discrepancies between the experimental and C766 RFs may in part be due to up to 28 % of T_1 not being accounted for in the DEMEC readings and the peak temperature drop T_1 not occurring at the height of 0.1L where the RF is calculated in C766.

3.4. Use of estimated temperatures in crack width calculation

This section compares the measured temperature rises in the walls with those determined using the spreadsheet provided in C766. The inputs to the spreadsheet include the binder content (in kg/m^3 of concrete), type (e.g. CEM1), pour thickness, placing and ambient temperatures, and type and thickness of insulation. Fig. 8 compares the measured and calculated values of T_1. In all but one case, T_1 is overpredicted by C766, with a maximum overprediction of 62 % for ICL5.

In light of the overestimate of temperature T_1 by C766, crack widths were recalculated with C766 and BS EN1992 using default input parameters from each document. The aim is to provide insight into the effect of these on calculated crack width since detailed material and temperature data are not commonly available at the design stage. The following input parameters were adopted:

- For indoor conditions the relative humidity was taken as either 50 % for BS EN 1992-1-1 (2004) or 45 % [4,9] for C766.
- T_1 was calculated with the C766 spreadsheet (see Fig. 8) [4].
- The CTE was taken as 10 με/°C for BS EN 1992-1-1 (2004) and in the case of C766, 9 με/°C for limestone aggregate, 13 με/°C for gravel and 12.5 με/°C [4,9] for sandstone.
- Concrete tensile strength and elastic modulus were calculated in terms of the measured 28 day concrete strength using Table 3.1 of BS EN 1992–1-1 (2004) [9].
- Shrinkage as per BS EN 1992-1-1 (2004)

Table 8
Predicted crack width and cracking risk, and observed crack width.

Test	w (test) LT	Predicted Crack Widths (mm)						Cracking Risk (CIRIA C766)	
		BS EN 1992-1-1 (2004)			CIRIA C766				
		$s_{r,max}$	EA	LT	$s_{r,max}$	EA	LT	EA	LT
ICL1	0	1013	0.16	0.26	1013	N/A	N/A (0.05)	0.96	0.89
ICL2	0.12	487	0.07	0.15	487	0.03	0.04	1.42	1.10
ICL3	0.1	487	0.08	0.16	487	0.03	N/A (0.03)	1.30	0.93
ICL4	0.04	1238	0.25	0.34	1238	0.09	0.10	1.26	1.14
ICL5	0.06	784	0.15	0.23	784	0.06	0.07	1.48	1.21
ICL6	0.38	1059	0.29	0.50	1059	0.15	0.22	2.23	2.48
ICL7	0.4	669	0.15	0.30	669	0.08	0.13	2.14	2.57
UoL1	0	784	0.11	0.15	784	N/A	NA (0.01)	0.88	0.55
UoL2	0	784	0.09	0.14	784	0.05	0.05	1.88	1.28
UoL3	0.14	784	0.18	0.25	784	0.10	0.10	2.26	1.41
UoL4	0.08	1300	0.23	0.38	1300	0.11	0.12	1.52	1.08
UoL5	0.10	1300	0.33	0.58	1300	0.18	0.22	1.98	1.41

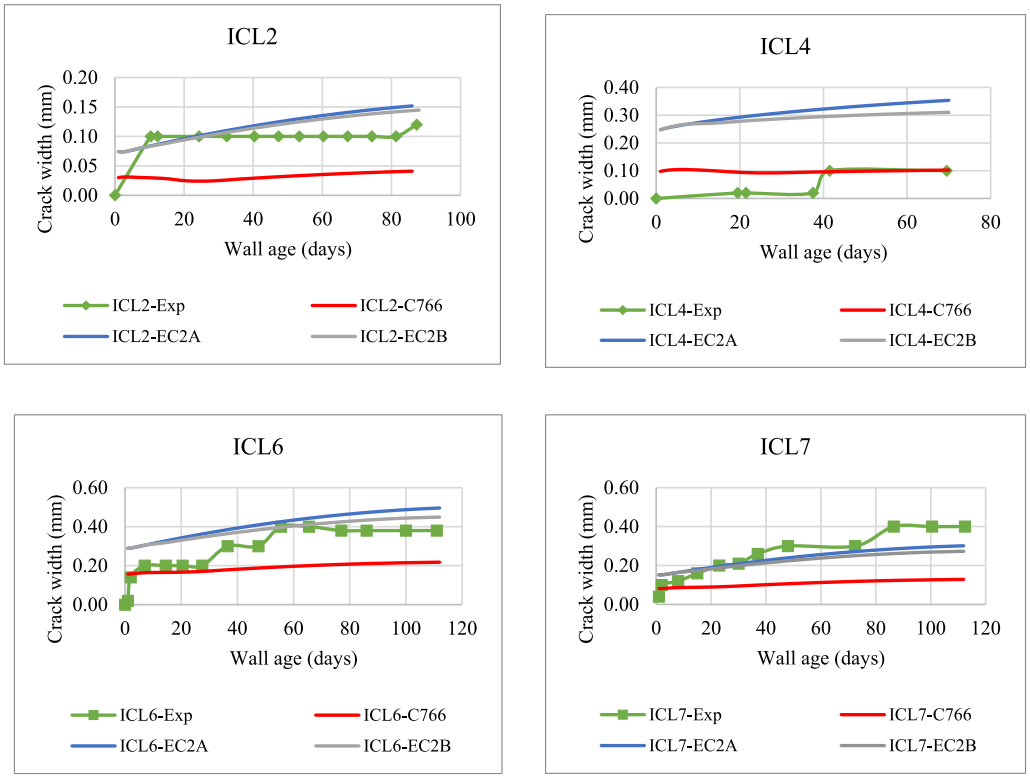

Fig. 7. Measured experimental crack width compared to guidance prediction.

Table 9
RF at EA and in the LT according to C766 and measured values.

Wall	$R_j(C766) = \frac{A_{old}E_{old}}{A_{new}E_{new} + A_{old}E_{old}}$		RF C766 at a height of 10%L including creep effects			RF measured heights of 8%L / 12.5%L		
	3 days	LT	3 days	1st cracking	LT	3 days	1st cracking	LT
ICL1	0.54	0.45	0.27	–	0.25	0.29/0.32	–	0.27/0.29
ICL2	0.60	0.51	0.30	0.28	0.25	0.25/0.16	0.27/0.18	0.47/0.37
ICL3	0.60	0.51	0.30	0.27	0.29	0.27/0.15	0.27/0.15	0.33/0.24
ICL4	0.60	0.51	0.30	0.28	0.28	0.30/0.12	0.29/0.12	0.29/0.14
ICL5	0.60	0.51	0.30	0.28	0.28	0.29/0.12	0.30/0.16	0.29/0.18
ICL6	0.68	0.60	0.34	0.34	0.30	0.46/0.43	0.38/0.18	0.60/0.60
ICL7	0.68	0.60	0.34	0.34	0.29	0.42/0.40	0.31/0.19	0.54/0.53
UoL1	0.54	0.45	0.27	–	0.25	0.54/0.64	–	0.27/0.17
UoL2	0.70	0.62	0.37	–	0.34	0.48/0.72	–	0.58/0.68
UoL3	0.70	0.62	0.37	0.33	0.34	0.59/0.61	0.27/0.27	0.22/0.21
UoL4	0.70	0.62	0.37	0.32	0.34	0.53/0.47	0.26/0.26	0.11/0.14
UoL5	0.70	0.62	0.37	0.33	0.33	0.36/0.30	0.40/0.35	0.59/0.54

Fig. 9 compares the resulting measured and calculated crack widths. Dependent on whether the input parameters are measured or estimated, the resulting crack widths are depicted 'experimental', or 'design'. Apart from the input parameters, the calculation method was unchanged. The crack spacing $s_{r,max}$ was calculated using equation 7.11. Fig. 9 shows that for all the walls except ICL6-7, the C766 crack widths increase when design rather than experimental input parameters are used. For BS EN 1992, crack widths calculated with design material parameters are in some cases less than calculated using experimental parameters due to i) the design CTE being an underestimate and ii) shrinkage being underestimated by BS EN 1992. C766 underestimated crack widths in ICL2, ICL3, ICL6, ICL7 and UoL3 with both measured and design input parameters. This was despite the horizontal reinforcement complying with the minimum requirements of C766. When taken with the findings of [18], this suggests that the calculation approach of C766 may be overly optimistic particularly if cracking occurs at early age as in ICL6-7. BS EN 1992 overestimates measured crack widths in all the walls apart from ICL6-7. The BS EN 1992 design prediction for ICL6 is good but the measured crack width is underestimated in ICL7. This is due to both the CTE and shrinkage strain being underestimated in the design calculation.

4. Conclusions

This paper compares maximum crack widths measured in 12 edge restrained walls with crack widths calculated with BS EN 1992 and C766. Seven of the walls were tested at ICL and five at UoL. The experimentally observed maximum restrained strain and maximum crack width occurred at a height of around 0.1L, where L is the wall length, above the base as suggested in C766. At ICL, the experimentally derived maximum RFs are similar to those calculated with C766 at early age and at first cracking. In walls which cracked significantly like ICL2, ICL6-7 the long-term RFs at the end of monitoring were significantly greater than at first cracking due to the inclusion of crack width in the

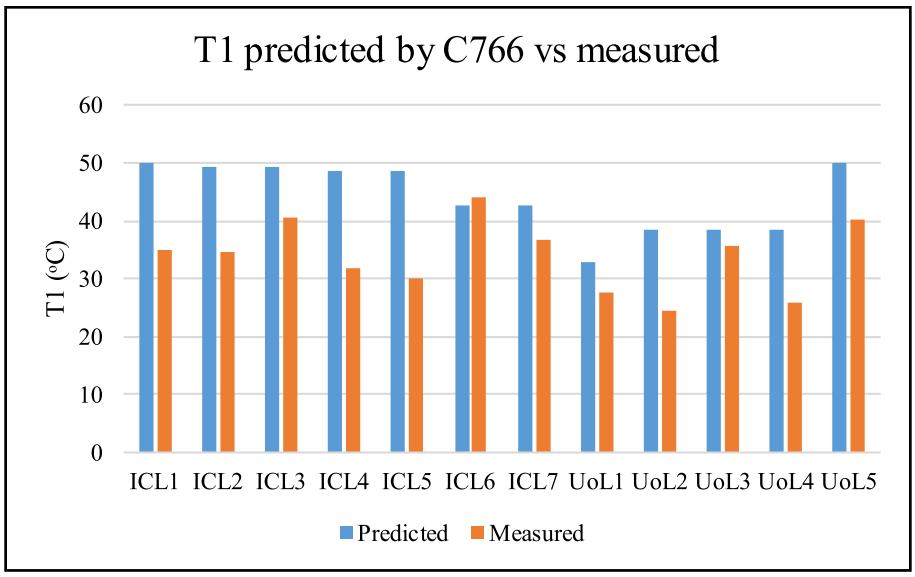

Fig. 8. Comparison of T_1 obtained with C766 calculator and experimental measurement.

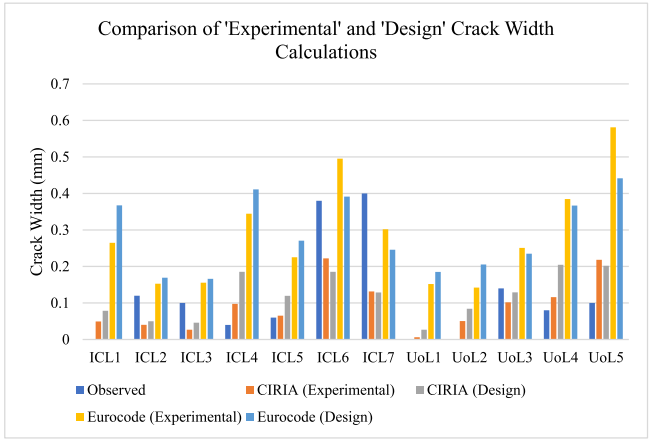

Fig. 9. Comparison of 'Experimental' and 'Design' crack width predictions.

calculation of restrained strain. At first cracking the experimentally determined RF in most walls was typically around 0.3 which is less than the default value of 0.5 adopted in BS EN 1992-3 (2006).

Nine of the walls cracked within the monitoring period. Walls ICL6-7 cracked at early age within 12 h of stripping the formwork. The early age cracks were widely spaced, through cracks. In ICL7, the width of the initial crack increased from 0.04 mm at first measurement to 0.40 mm at end of monitoring at 113 days. Over time, further cracking developed in ICL6-7. These cracks were relatively narrow and short in length. In the other walls, cracking occurred between 7 and 50 days after stripping the formwork due restraint of combined early age thermal and shrinkage strain. These cracks tended to develop in short unconnected lengths, which subsequently joined forming wider cracks that extended over the wall height.

Crack widths were initially calculated using measured material properties and temperature drop T_1. BS EN 1992 provided an upper-bound to the measured crack widths for all the walls, apart from ICL7, while CIRIA C766 underestimated the maximum crack widths in five of the 12 walls. The underestimate ranged between 42 and 80 % and was greatest for walls ICL6-7 where early age cracking developed within 12 h of stripping the formwork.

The temperature drop, T_1, predicted by C766 was compared with the maximum measured temperature drop for each wall and found to be up to 62 % higher than measured. Crack widths were recalculated with both C766 and BS EN 1992 using design material properties, derived from the measured 28 day concrete strength, and T_1 from C766. These crack widths, depicted "design" were typically greater than calculated using measured input parameters. The design C766 crack widths were less than the maximum measured crack widths in walls ICL2, ICL3, ICL6, ICL7 and UoL3. The underestimate in calculated crack width does not appear to be related to the reduction of minimum reinforcement area in C766 since the horizontal reinforcement in walls ICL2, ICL3 and ICL7 complied with the more onerous requirements of BS EN 1992-1-1 (2004) by a significant margin. BS EN 1992 gave conservative estimates of crack width in all the walls except ICL7. In conclusion, the use of C766 may pose a risk of underestimating maximum crack width. The reasons for this are the subject of ongoing research.

Declaration of Competing Interest

The authors declare that they have no known competing financial interests or personal relationships that could have appeared to influence the work reported in this paper.

Acknowledgements

The authors kindly acknowledge financial support from the Engineering and Physical Sciences Research Council (EPSRC) under grants EP/T004142/1 and EP/T004185/1, titled "Understanding the cracking behaviour of reinforced concrete elements subjected to the restraint of imposed strains."

References

[1] Øyvind Bjøntegaard (Norwegian Public Roads Administration), "COIN Project report no 31: Basis for and practical approaches to stress calculations and crack risk estimation in hardening concrete structures – State of the art," Blindern, 2011. [Online]. Available: www.coinweb.no.

[2] EUROPEAN COMMITTEE FOR STANDARDIZATION, "FprEN 1992-1-1. Eurocode 2: Design of concrete structures - Part 1-1: General rules - Rules for buildings, bridges and civil engineering structures," Brussels, 2022.

[3] RILEM Technical Committee TC-242-MDC, "RILEM draft recommendation: TC-242-MDC multi-decade creep and shrinkage of concrete: material model and structural analysis*: Model B4 for creep, drying shrinkage and autogenous shrinkage of normal and high-strength concretes with multi-decade applicability," *Materials and Structures/Materiaux et Constructions* 2015; 48(4): 753–70, doi: 10.1617/s11527-014-0485-2.

[4] Bamforth P, Control of cracking caused by restrained deformation in concrete. London: CIRIA C766; 2018.

[5] Bamforth P, "Concreting large-volume (mass) pours," in *Construction of deep lifts and large volume pours*, London: CIRIA, 1995.
[6] Shehzad MK, Forth JP, Bradshaw A. Imposed loading effects on reinforced concrete walls restrained at their base. Proc Inst Civ Eng - Struct Build 2020;173(6):413–28.
[7] Micallef M, Vollum RL, Izzuddin BA. Cracking in walls with combined base and end restraint. Mag Concr Res 2017;69(22):1170–88. https://doi.org/10.1680/jmacr.17.00026.
[8] Beeby W, Forth JP. Control of cracking in walls restrained along their base against early thermal movements. Concr Transp Infrastruct 2005:123–32.
[9] Schlicke D, Dorfmann EM, Fehling E, Tue NV. Calculation of maximum crack width for practical design of reinforced concrete. Civ Eng Des 2021;3(3):45–61. https://doi.org/10.1002/cend.202100004.
[10] British Standards Institution, "Eurocode 2: Design of concrete structures-Part 1-1: General rules and rules for buildings," 2004.
[11] British Standards Institution., Eurocode 2 : design of concrete structures. Part 3, Liquid retaining and containment structures. BSI, 2006.
[12] CEN, "EN 1992-1-1: Eurocode 2: Design of concrete structures - Part 1-1: General rules and rules for buildings," 2004.
[13] Gilbert RI. Cracking Caused by Early-age Deformation of Concrete-Prediction and Control. In: Procedia Engineering. Elsevier Ltd; 2017. p. 13–22. https://doi.org/10.1016/j.proeng.2017.02.012.
[14] ACI Committee 207, *Effect of restraint, volume change and reinforcement of cracking of mass concrete*, 207.2R–95.
[15] Beeby AW. The prediction of crack widths in hardened concrete. Struct Eng 1979;57A(1).
[16] Kanstad T, Klausen A, Menga A. "Background document to prEN1992-1-1 D7 Rev 7 Annex D: Evaluation of Early-Age and Long-Term Cracking Due to Restraint," Norway, 2021.
[17] Bamforth PB. "Early-age thermal crack control in concrete," London: CIRIA C660, 2007. [Online]. Available: www.ciria.org.
[18] Micallef M, Vollum RL, Izzuddin BA. Crack development in transverse loaded base-restrained reinforced concrete walls. Eng Struct 2017;143:522–39. https://doi.org/10.1016/j.engstruct.2017.04.035.
[19] Jędrzejewska A, Kanavaris F, Zych M, Schlicke D, Azenha M. Experiences on early age cracking of wall-on-slab concrete structures. Structures 2020;27:2520–49. https://doi.org/10.1016/j.istruc.2020.06.013.
[20] Shen D, Liu Ci, Wen C, Kang J, Li M, Jiang H. Restrained cracking failure behavior of concrete containing MgO compound expansive agent under adiabatic condition at early age. Cem Concr Compos 2023;135:104825. https://doi.org/10.1016/j.cemconcomp.2022.104825.
[21] Zapata-Padilla JR, et al. Portland cement-based grouts enhanced with basalt fibers for post-tensioned concrete duct filling. Materials 2023;16(7):2842. https://doi.org/10.3390/ma16072842.
[22] Elwakeel A, Shehzad M, El Khoury K, Vollum R, Forth J, Izzuddin B, et al. Assessment of cracking performance in edge restrained RC walls. Struct Concr 2022;23(3):1333–52. https://doi.org/10.1002/suco.202100688.
[23] Shen D, Liu C, Jiang J, Kang J, Li M. Influence of super absorbent polymers on early-age behavior and tensile creep of internal curing high strength concrete. Constr Build Mater 2020;258:120068. https://doi.org/10.1016/j.conbuildmat.2020.120068.
[24] Fédération internationale du béton., *Model code 2010 : final draft*. International Federation for Structural Concrete (fib), 2012.
[25] P. B. chair) RILEM Technical Committee TC-242-MDC (Zdeněk, "RILEM draft recommendation: TC-242-MDC multi-decade creep and shrinkage of concrete: material model and structural analysis*: Model B4 for creep, drying shrinkage and autogenous shrinkage of normal and high-strength concretes with multi-decade applicability," *Materials and Structures/Materiaux et Constructions* 2015; 48(4): 753–70, 2015, doi: 10.1617/s11527-014-0485-2.
[26] American Concrete Institute. and ACI Committee 209\mathord{-} Creep and Shrinkage., *Guide for modeling and calculating shrinkage and creep in hardened concrete*. American Concrete Institute, 2008.